frontiers | Frontiers in Biomaterials Science

TYPE Original Research
PUBLISHED 15 July 2024
DOI 10.3389/fbiom.2024.1408748

OPEN ACCESS

EDITED BY
Monica Boffito,
Polytechnic University of Turin, Italy

REVIEWED BY
Santosh Phuyal,
University of Oslo, Norway
Sharda Yadav,
Griffith University, Australia
Qiang Wei,
Sichuan University, China

*CORRESPONDENCE
Silviya Petrova Zustiak,
silviya.zustiak@slu.edu

RECEIVED 28 March 2024
ACCEPTED 24 June 2024
PUBLISHED 15 July 2024

CITATION
Ferchichi E, Stealey S, Bogert P and Zustiak SP (2024), Tunable gelatin methacrylate polyethylene glycol diacrylate hydrogels for cell mechanosensing applications.
Front. Biomater. Sci. 3:1408748.
doi: 10.3389/fbiom.2024.1408748

Tunable gelatin methacrylate polyethylene glycol diacrylate hydrogels for cell mechanosensing applications

Eya Ferchichi, Samuel Stealey, Paige Bogert and Silviya Petrova Zustiak*

Department of Biomedical Engineering, School of Science and Engineering, Saint Louis University, St Louis, MO, United States

Three-dimensional (3D) tissue-engineered scaffolds mimic the physiological environment of cells by providing essential structural support, biochemical cues, and the mechanical strength needed for cell adhesion, proliferation, migration, and differentiation. Hydrogels like polyethylene glycol diacrylate (PEGDA) are commonly used biomaterials for cell culture due to their affordability, tunable stiffness, and ability to efficiently transport nutrients and gases. However, PEGDA lacks cell adhesion sites essential for cell proliferation and migration and has limited degradability. Methacrylated gelatin (GelMA) produced from denatured bovine collagen, crosslinks under ultraviolet light (UV) resulting in a degradable hydrogel with cell adhesion sites. Here, we synthesized GelMA with variable degree of methacrylation and crosslinked it with PEGDA to produce cell scaffolds with independently tunable mechanical and biochemical properties by varying the ratios of the two polymers. We determined polymer ratios that resulted in scaffolds with different mechanical properties but the same gelatin concentrations (providing cell adhesion and degradation sites) as well as different gelatin concentrations but the same mechanical properties. With the developed scaffold library, we further used a design of experiments approach to probe the parameter space and perform detailed analysis on chemical composition-scaffold properties as well as scaffold properties-cell behavior correlations. Our findings showed that hydrogel properties such as modulus, swelling, pore size, and permeability, strongly depended on total polymer concentration and not on the GelMA fraction. GelMA significantly influenced cell spreading, while addition of any amount of PEGDA delayed cell spreading significantly. We suggest that such analysis will broaden the utility of the GelMA/PEGDA hydrogels, presenting a versatile platform for mechanosensing research in 3D environments.

KEYWORDS

cell scaffold, mechanosensing, mechanobiology, stiffness, compliance, hydrogel

1 Introduction

The extracellular matrix (ECM) is a complex 3D network composed of proteins and other molecules that surround cells in tissues throughout the body (Theocharis et al., 2016). The ECM includes structural proteins such as collagen, elastin, and fibronectin, as well as proteoglycans and glycosaminoglycans that form a hydrated gel-like substance (Lepedda et al., 2021). Decades ago, research revealed that the ECM supports and regulates cell growth and behaviors (Kim et al., 1999; Dutta and Dutta, 2009). It provides physical support to cells, allows for cellular movement and communication, and regulates cell signaling and

behavior, which makes it crucial for physiological processes such as tissue repair and regeneration as well as pathological processes such as cancer metastasis, fibrosis, and inflammation (Walker et al., 2018). Since then, multiple studies have focused on developing physiologically relevant 3D hydrogel microenvironments that mimic the structure, properties, and function of the native ECM (Tibbitt and Anseth, 2009). Cell–scaffold interactions and scaffold mechanical properties are essential for cell fate and for the regulation of cellular behavior (Caliari and Burdick, 2016). Thus, the chemical composition of the scaffold is an important factor in biomaterial development because it dictates the material physical, mechanical, and biochemical properties. These material properties in turn, influence cell survival, spreading, proliferation, migration, and differentiation (Kim et al., 1999; Dutta and Dutta, 2009; Huang et al., 2017).

Gelatin, which is denatured collagen, is naturally found in most tissues which makes it an excellent biomaterial for many applications. Gelatin promotes cell adhesion and proliferation due to the presence of cell-binding domains such as the arginine-lysine-aspartate (RGD) sequence that interacts with cell surface receptors (Hoch et al., 2012; Huang et al., 2017). To address the limitations of using gelatin alone, Van Den Bulk et al. (2000) chemically modified gelatin with methacrylic anhydride by substituting the available amino groups with methacrylate functional groups and obtained gelatin methacrylate, also referred to as methacryloyl (GelMA). GelMA has since become widely used in tissue engineering and regenerative medicine due to its easy-to-use crosslinking chemistry, stability under physiological conditions, and support of cell attachment (Van Den Bulcke et al., 2000; Hoch et al., 2012; Loessner et al., 2016; Huang et al., 2017; Sun M. et al., 2018). GelMA has been shown as an excellent scaffold for mechanosensing applications in particular, because the polymer fibers possess both high deformability and modulus, which maximize cell adhesive forces due to fiber recruitment (Dong et al., 2024). The addition of methacrylate groups to the gelatin backbone enables gelatin to undergo photocrosslinking in response to light exposure, which can be used to control the properties (e.g., mechanical and biochemical) of the resulting hydrogel (Loessner et al., 2016). However, to achieve diverse mechanical properties one has to either: i) modify the degree of methacrylation, which offers somewhat limited tunability due to the finite number of modifiable groups (Pepelanova et al., 2018; O'Connell et al., 2018), ii) adjust the UV exposure resulting in uncoupled reactive groups and with possible implications for cell function due to UV exposure (O'Connell et al., 2018), or iii) modify the polymer concentration (Sun Y. et al., 2018), which leads to both increase in mechanical and biochemical properties (i.e., prevents independent tunability) and could also result in an impractically viscous precursor solution. Hence, a different strategy might be desired for achieving GelMA hydrogels with varying properties, such as mechanical and biochemical, for use in applications such as mechanosensing.

The objective of this study was to assess the utility and explore the structure-property relationships for GelMA/poly (ethylene glycol) diacrylate (PEGDA) hydrogel scaffolds for mechanosensing applications. The addition of PEGDA introduces key features: modulation of mechanical properties independently of biochemical ones for mimicking native tissue mechanics and enhanced hydrophilicity for a well-hydrated microenvironment conducive to cell survival (Hutson et al., 2011). Further, while others have shown changes in porosity and pore size with PEGDA addition, the GelMA/PEGDA gels have been shown to retain their porous structure (Mamaghani et al., 2018; Wang et al., 2018), facilitating nutrient and oxygen diffusion while aiding in waste product removal. This mass transport is crucial for supporting cell viability and functionality within the 3D hydrogel matrix.

GelMA/PEGDA hydrogels, compared to GelMA-only hydrogels, demonstrate enhanced mechanical properties and prolonged degradation rates of up to several weeks (Xiao et al., 2019a), making them suitable for prolonged cell mechanosensting studies (Jiang et al., 2019). For example, *in vitro* experiments have shown that osteoblasts adhere and proliferate effectively on the hydrogels' surface, indicating excellent cell viability and biocompatibility and positioning the GelMA/PEGDA hydrogel as a suitable material for guided bone regeneration applications (Wang et al., 2018). GelMA/PEGDA hydrogels have also been utilized in 3D *in vitro* models of intestinal mucosa, accurately mimicking the intestinal barrier's function and permeability, thus enabling predictions of drug absorption and understanding intestinal function related diseases (Vila et al., 2020). Another study showed breast cancer cells seeded in GelMA/PEGDA hydrogels formed either spherical tumor-like clusters or exhibited spindle-shaped morphology, indicative of invasive behavior, where cell spreading was guided primarily by the GelMA content (Peter et al., 2019).

Because many recent studies have shown the utility of the GelMA/PEGDA hydrogels as cell scaffolds (Hutson et al., 2011; Duan et al., 2022), here we sought to perform detailed structure-property analysis of the hydrogels and their effect on cell spreading, viability, and drug responsiveness. Our detailed analysis focused on the effect of total polymer content as well as GelMA fraction (correlating with number of adhesive sites and enzymatic gel degradability) on the gels' mechanical and physical properties (i.e., modulus, swelling, pore size, and permeability) and subsequently the effect of those properties on cell viability, spreading and drug responsiveness over 7–14 days of culture. Through varying the PEGDA and GelMA concentrations, we were able to identify gel conditions with the same modulus but different number of adhesive ligands and different modulus but the same number of adhesive ligands, positioning the GelMA/PEGDA gels as excellent scaffolds in mechanosensing applications.

2 Materials and methods

2.1 Materials

Poly (ethylene glycol) diacrylate (PEGDA, MW 5,000 g/mol) was obtained from Laysan Bio, Inc (Arab, AL). Gelatin from bovine skin type B (bloom strength 257), methacrylic anhydride (MAA), trypsin, ethylenediaminetetraacetic acid (EDTA), and Ribonuclease A (RNase) were obtained from Millipore Sigma (St. Louis, MO). Phosphate buffered saline (PBS), Atto 655-NHS ester, fluorescence dye removal columns, and SnakeSkin™ dialysis tubing (10K MWCO) were obtained from ThermoFisher Scientific (Waltham, MA). Irgacure 2,959 was obtained from BASF Corporation (Florham Park, NJ) and silicone spacers were obtained from Grace Bio-Labs (Bend, OR). Roswell Park Memorial Institute (RPMI) 1,640 medium and fetal bovine serum (FBS) were obtained from Hyclone (Logan,

UT). Penicillin/streptomycin (pen/strep) was obtained from MP Biomedicals (Santa Ana, CA). Propidium iodide (PI), acridine orange (AO), Cell Tracker Green CMFDA Dye, dimethyl sulfoxide (DMSO), temozolomide (TMZ), and four-chambered coverglass were obtained from Fisher Scientific (Hamptom, NH). U-87 human glioblastoma and NIH 3T3 fibroblast cells were obtained from American Type Culture Collection (Manassas, VA).

2.2 GelMA preparation

GelMA of low and high degree of modification (DM) was synthesized following a protocol developed by Van Den Bulcke et al. (Van Den Bulcke et al., 2000) with some modifications. Briefly, 5 g gelatin was dissolved by gently mixing it in 50 mL of 1X PBS pH 7.4 at 60 °C. After the gelatin was fully dissolved, MAA was added (2.50 mL for the high DM and 0.25 mL for the low DM GelMA) dropwise via a syringe pump at a rate of 0.5 mL/min under vigorous stirring (500 rpm). For the high DM, a 1:10 M ratio of free amine groups in gelatin to MAA was used and for the low DM, a 1:1 M ratio was used. The molar concentration of amine groups was assumed to be 0.335 mmol amine groups per gram of gelatin as determined previously by Ven Den Bulcke et al. (Van Den Bulcke et al., 2000) for bovine gelatin (type B) with bloom strength of 257 (the gelatin used here). After 2 h of reaction under stirring at 60 °C, 250 mL of PBS was added to neutralize the reaction. The mixture was dialyzed for 7 days against deionized water at 50 °C using 10K MWCO dialysis tubing with daily change of the dialysate buffer, then lyophilized for 5 days. The collected GelMA powder was stored at −20 °C until use.

To confirm the successful methacrylation of gelatin and quantify the DM, ^{1}H-nuclear magnetic resonance (NMR) spectroscopy was used. For the analysis, 0.8 mg of GelMA or gelatin was dissolved in 600 µL deuterium oxide and analyzed on a HDTM 700 MHz NMR spectrometer (Bruker, Billerica, MA). The DM was defined as the percentage of lysine methylene groups (2.8–2.95 ppm) of the gelatin that were modified in the GelMA (Hoch et al., 2012). The ^{1}H NMR spectra were normalized to the signal at 0.8 ppm corresponding to the proton of the methyl group. DM was calculated from the integration of the ^{1}H-NMR spectra to determine the area, A, of the lysine signal in both GelMA and gelatin as:

$$DM\,(\%) = 1 - [A\,(lysine\,methylene\,of\,GelMA)/ (A\,(lysine\,methylene\,of\,gelatin) \times 100 \quad (1)$$

2.3 GelMA/PEGDA hydrogel fabrication

Stocks solution of PEGDA and lyophilized high or low DM GelMA were made by gently mixing each polymer in PBS at 30% w/v until both polymers were completely dissolved. High DM was used for all experiments unless specified otherwise. The hydrogels were prepared by radical crosslinking of different ratios of GelMA and PEGDA in the presence of the photoinitiator Irgacure 2959 at 0.1% w/v final concentration. Irgacure 2959 (<2 wt% at 25 °C water solubility (Tomal and Ortyl, 2020) stock solution was first prepared at 1% w/v in deionized (DI) water via sonication for 8 h and stored up to 14 days under constant stirring and protected from light.

TABLE 1 Hydrogel composition and abbreviations used.

Abbreviation	GelMA [% w/v]	PEGDA [% w/v]
G2P3	2	3
G2P5	2	5
G2P10	2	10
G5P2	5	2
G5P5	5	5
G5P10	5	10
G10	10	0
G10P2	10	2
G10P5	10	5
G10P10	10	10

Table 1 summarizes the different concentrations of GelMA and PEGDA used and the associated hydrogel abbreviations. Dissolved GelMA and PEGDA were mixed and diluted in PBS to the desired final concentration. Once Irgucure 2959 was added, the solution was placed between two glass plates with two silicone spacers (1 mm thickness) and placed under 365 nm UV light for 10 min at 10 cm distance to the UV light (4.81 mW/cm^2) to form a gel.

2.4 Rheology and swelling ratio

Rheological measurements were performed using an AR-2000ex rheometer (TA Instruments, New Castle, DE) with a 20 mm parallel plate geometry. Storage modulus, G', and loss modulus, G'', were measured at a constant strain of 0.1%, which was within the linear viscoelastic region of all hydrogels tested, at a frequency of 1–10 Hz and an axial force of 0.2 N (Vila et al., 2020). For testing, 500 µL gels of 1 mm thickness were equilibrium swollen for 24 h at room temperature in DI water and cut into 20 mm discs. Before measurements, excess water from the gel surface was wicked away carefully using KimWipe. The measured G' was converted to Young's modulus, E, using the following equation:

$$E = G'2\,(1 + \upsilon) \quad (2)$$

where υ is the Poisson's ratio which was approximated to 0.5 for the GelMA/PEGDA hydrogels.

For swelling ratio measurements, hydrogels were prepared as 6 mm × 1 mm slabs and equilibrium swollen in DI water for 24 h at 37 °C. Their swollen mass (M_s) was measured. Hydrogels slabs were then dried for 24 h at 60 °C to obtain the dry mass (M_d). The swelling ratio (Q_M) was calculated as the ratio of M_s to M_d (M_s/M_d).

2.5 Scanning electron microscopy

Hydrogels were soaked in DI water overnight and were then frozen at −80 °C for 30 min and lyophilized for 24 h. The samples were sputter coated with gold for 240 s at 20 mA (SCD 005, BAL-TEC, Liechtenstein). The samples were imaged via Scanning

Electron Microscopy (SEM, EVO LS15) under high vacuum at ×5 kV and ×500 magnification. Pore size and wall thickness were measured using ImageJ software (50 pores were measured per image from three images per hydrogel type).

2.6 Fluorescence correlation spectroscopy

Fluorescence correlation spectroscopy (FCS) was used to investigate the effect of polymer concentration on hydrogel mesh size and diffusivity. Ribonuclease A (RNase A) was used as a model protein and was fluorescently labeled with Atto 655-NHS ester, according to the manufacturer's protocol. Briefly, Atto 655-NHS ester and RNase were dissolved in PBS and reacted under gentle mixing for 2 h while protected from light to avoid photobleaching. Unbound dye was removed using dye removal columns with >95% removal efficiency. Labeling efficiency was measured to be 64% and was calculated by measuring the bound fraction of Atto 655 using a two-component autocorrelation function fit. Next, fluorescently labeled RNase was added to hydrogels of varying GelMA and PEGDA concentration by mixing with the hydrogel precursor solution for a final RNase concentration of 1 μg/mL. Gels were placed in an 8-chambered coverglass, crosslinked as previously described and swollen in a solution of 1X PBS with 1 μg/mL fluorescent RNase to maintain constant protein concentration within each hydrogel.

FCS measurements were performed using Microtime 200 software (PicoQuant, Berlin, Germany). Atto 655-NHS ester (0.2 nM) in PBS was used to calibrate the illuminated confocal volume. A 640 nm ps pulsed laser was used at an optical power of 11 μW for at least five measurements of 120 s for each sample. An autocorrelation function $G(\tau)$ was obtained for each measurement:

$$G(\tau) = \frac{1}{N}\frac{1}{\left[1+\left(\frac{\tau}{\tau_D}\right)\right]}\frac{1}{\left[1+p\left(\frac{\tau}{\tau_D}\right)\right]^{0.5}} \quad (3)$$

where N is the number of fluorescent particles, $p = r_o/z_o$ is an instrumental constant, r_o is the radius and z_o is the axial length of the focused laser beam spot, and τ_D is the solute diffusion time. A one component autocorrelation function fit was used for all samples as protein interaction with the polymer was not expected. Additionally, a triplet model was used to account for possible excitation of molecular triplet states at higher laser intensities. Autocorrelation functions for labeled RNase A were normalized as follows:

$$\text{Normalized } G(\tau) = \frac{(G(\tau_D))}{(G(\tau 0))} \quad (4)$$

where $G(\tau_D)$ is the value of Eq. (3) at each time point and $G(\tau_0)$ is the value of Eq. (3) at the initial time point.

2.7 Cell maintenance

Human glioblastoma cells U87 were cultured in RPMI-1640 medium supplemented with 10% v/v FBS and 1% v/v pen/strep in a humidified incubator at 37 °C and 5% CO_2 in a T-75 flask. NIH 3T3 cells were cultured in DMEM medium supplemented with 10% FBS and 1% pen/strep in a humidified environment at 37 °C and 5% CO_2 in a T-75 flask. Once at 80% confluency, cells were harvested with 0.1 M Trypsin/EDTA at an exposure time of 5 min and used for experiments. Only cells between passages 10 and 14 were used for experiments.

2.8 Cell encapsulation in GelMA/PEGDA hydrogels

For cell encapsulation, hydrogels were prepared as described above except that cells were added to the gel precursor solution at a concentration of 10^6 cells/mL. Then, 20 μL hydrogel precursor solution droplets were pipetted between two glass plates separated by 1 mm silicone spacers and placed under UV light (365 nm) for 10 min at 10 cm distance from the light. The hydrogels containing encapsulated cells were cultured in a humidified incubator at 37 °C and 5% CO_2 for up to 14 days with a change in media every other day.

2.9 Cell viability measurement

Live/dead (AO/PI) staining was used to assess cell viability. At specified time points, hydrogel encapsulated cells were incubated with PI (2 μg/mL) and AO (2 μg/mL) for 30 min, rinsed with PBS and soaked in complete cell culture medium for imaging. Images were taken using a confocal microscope (Leica Confocal SP8, Leica Microsystems, Wetlzar, Germany) at ×10 magnification. Cell viability was calculated using a MATLAB code that counts individual cells stained with AO (all cells) and with PI (dead) and then calculates the ratio:

$$\text{Viability } (\%) = \frac{\#\text{ of all cells } - \#\text{ of dead cells}}{\#\text{ of all cells}} * 100\% \quad (5)$$

2.10 Drug screening

For drug screening, U87 cells were first encapsulated in the hydrogels at a density of 10^6 cells/mL and cultured for 3 days in a 48-well plate. On day 3, the encapsulated cells were treated with 0, 1, 2, 3, and 4 mM TMZ in 4% DMSO and incubated for an additional 3 days. On the third day following TMZ addition, cells were stained with 2 μg/mL PI (dead cells) and 1 μM Cell Tracker Green (live cells) for 30 min at 37 °C. Z-stack images were captured using a Leica SP8 confocal microscope at ×10 magnification. Cell viability was calculated for each hydrogel condition and TMZ concentration as previously described.

2.11 Quantification of number of cells spreading

To assess cell spreading, cells encapsulated in GelMA/PEGDA hydrogels were stained with Cell-Tracker Green at a concentration of 1 μM for 30 min at 37 °C. The staining medium was then exchanged with fresh complete medium. Images were captured using a confocal microscope at ×10 and ×20 magnification and

analyzed on ImageJ via the Shape Descriptor and Area software plug-ins. For the four conditions G2P3, G10, G10P2, and G10P10, cell spreading area was determined by generating a mask to delineate the perimeter of each individual cell. Cell shape (circularity) was then calculated from the following relationship:

$$\text{Shape factor} = \frac{4\pi(\text{area})}{\text{Perimeter}^2} \quad (6)$$

Circularity was measured on a scale of 0–1, where values of 0.6-1 were taken to designate rounded cells and values of 0–0.5 were taken to designate elongated cells. Cell spreading was also quantified for all hydrogel types by assessing the number of cells that were spreading (had protrusions and were not round in shape) to the total cell count in the image. Analysis involved examining >100 cells for each data point across a minimum of three independent experiments. However, for G10P10 gels, analysis was based on >30 cells from three separate experiments due to the low cell number in these gels.

2.12 Dynamic data visualization with JMP

JMP (version 16.0.0) statistical software (SAS Institute, Cary, NC) was used for dynamic data visualization as well as statistical analysis. We leveraged the software's capabilities to generate contour plots, allowing us to effectively visualize trends and patterns within our data. Contour plots assist in identifying regions of interest, boundaries, or thresholds where specific outcomes occur or where variables exhibit notable changes. To derive regression models and obtain predictive expressions, we employed the method of least squares within JMP. This statistical technique was applied with default emphasis on effect leverage. By emphasizing effect leverage, we aimed to prioritize influential factors and better understand their impact within our experimental setup. By weighing these influential factors, we aimed to enhance the robustness of our models and better understand variable relationships in our analyses conducted using JMP.

2.13 Statistics

GraphPad Prism software was used to express results as average ± standard deviation (SD) from three independent experiments, where 3–10 samples were used per experiment. Multiple groups were compared using single factor analysis of variance (ANOVA) with a Tukey's *post hoc* test. Two-tailed Student's t-test was used to compare between two groups. A value of $p < 0.05$ was considered significant. The coefficient of variance (%CV) was calculated as the standard deviation divided by the mean.

3 Results

3.1 Methacrylation of gelatin

Here, we synthesized GelMA with varying degrees of methacrylation. In this process, the amino groups in gelatin are functionalized through methacrylation using methacrylic anhydride (MAA), resulting in the formation of GelMA. Upon exposure to UV light in the presence of a photoinitiator, the methacrylate groups within GelMA can covalently bond, resulting in the crosslinking of GelMA chains and the formation of a stable hydrogel. This study followed a protocol established by Van den Bulcke et al. (Van Den Bulcke et al., 2000) with the degree of methacrylation adjusted by controlling the quantity of MAA, as illustrated in Figure 1A. ^{1}H NMR spectroscopy confirmed the methacrylation (Figure 1B). The NMR signal at 1.9 ppm corresponds to the methylene protons (CH_2) adjacent to the carbonyl group of the methacrylate and the signals at 5.4 and 5.7 ppm correspond to the protons of the vinyl group (CH = CH_2) in the methacrylate (Van Den Bulcke et al., 2000). The lysine signal at 2.9 ppm, highlighted in green, nearly disappeared when using higher molar ratios of MAA to gelatin but changed only minimally for the lower molar ratio of MAA to gelatin (Yue et al., 2015; Claaßen et al., 2018). We calculated 80% degree of methacrylation for the high DM GelMA and 16% degree of methacrylation for the low DM GelMA. GelMA with a high DM was used for subsequent experiments unless otherwise indicated.

3.2 Mechanical and physical properties of GelMA and GelMA/PEGDA hydrogels

We used a combination of GelMA and PEGDA polymers to fabricate hydrogels with different stiffness, as governed primarily by the PEGDA concentration, or different biochemical composition (e.g., RGD and MMP moieties), as governed primarily by the GelMA concentration. We tested various ratios of GelMA/PEGDA hydrogels as follows: 2%, 5%, and 10% w/v GelMA combined with 0%, 2%, 3%, 5%, and 10% w/v PEGDA (Table 1). We tested GelMA alone as a control, but not PEGDA alone as it lacks binding sites for cell attachment and spreading. The chosen compositions were based on prior literature (Mahdavi et al., 2021; Liu et al., 2024) as well as on our preliminary work establishing the lower and upper polymer concentration boundaries. For example, G10P10 was the highest concentration used because the hydrogel precursor solution became too viscous to pipette at higher polymer concentrations. G10 was the only control tested because G2 did not gel and G5 resulted in a very soft gel, which was difficult to handle. Similarly, G2P3 was used instead of G2P2, as G2P2 did not gel. Hence, G2P3 was the lowest and G10P10 the highest practical polymer concentration which resulted in a stable hydrogel that was easy to handle. These compositions resulted in a range of stiffness from Young's modulus of ~3.7 kPa–~45.0 kPa (Figures 2A–C). Overall, within each group (for the same GelMA concentration), Young's modulus increased with an increase in PEGDA concentration. Furthermore, we were able to fabricate gels with the same stiffness but different biochemical properties as well as gels with the same biochemical properties but different stiffness. Specifically, we fabricated both soft and stiff gel pairs with the same Young's modulus but varying biochemical composition due to different GelMA concentration: soft G2P3 and G10 gels (Young's modulus of ~4 kPa) and stiff G2P10 and G10P10 gels (Young's modulus of ~30 kPa). At the same time, we achieved gels with the same biochemical properties (i.e., GelMA concentration) but varying Young's modulus (e.g., G2P3 vs. G2P10 and G10 vs. G10P10). We also noted that hydrogel swelling showed inverse

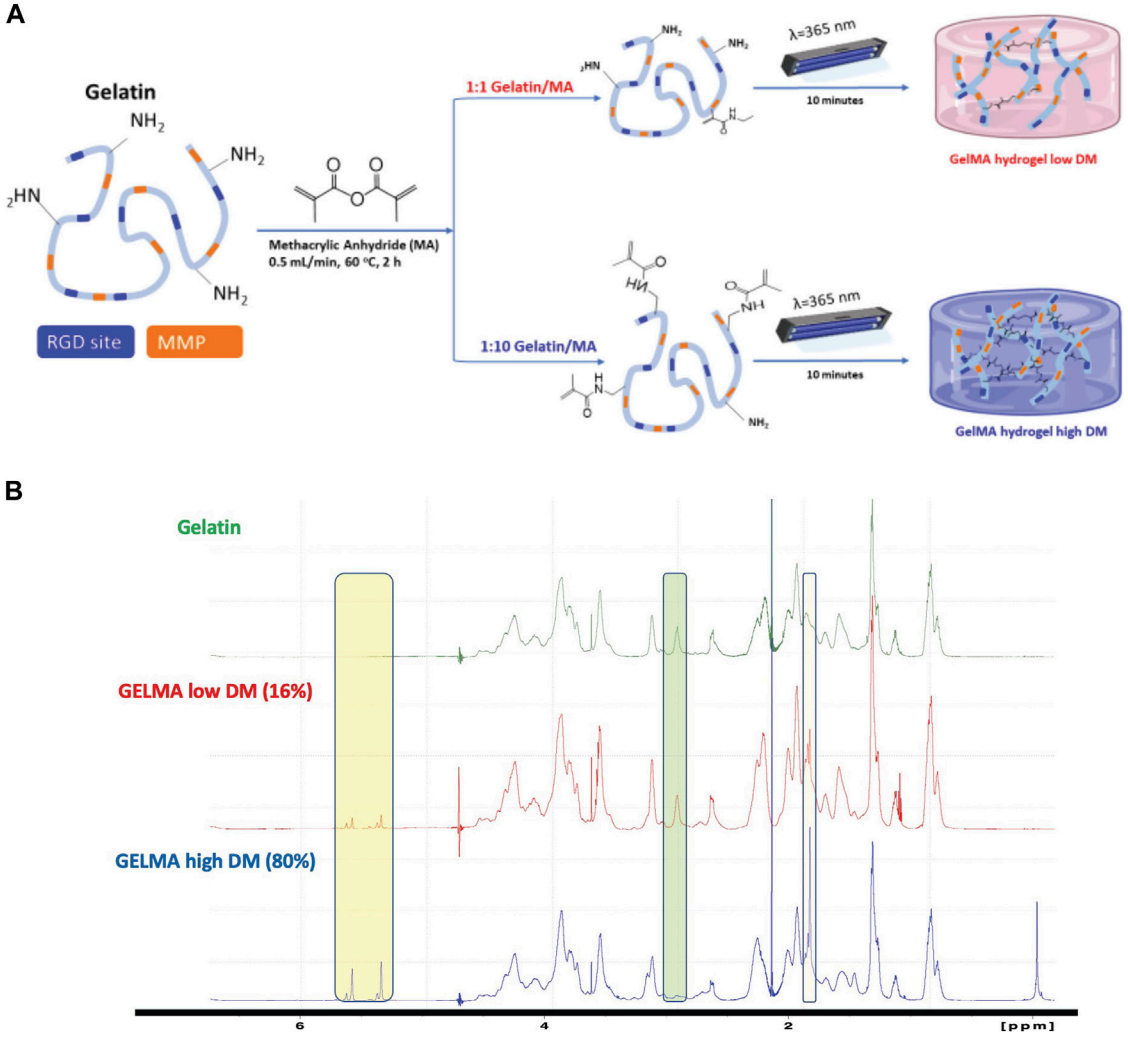

FIGURE 1
(A) Synthesis of GelMA. High and low degree of modification (DM) of the amino groups on gelatin with MAA to form GelMA without affecting the RGD adhesion and MMP degradation moieties. **(B)** ^{1}H-NMR spectra for gelatin and GelMA with high and low DM. Yellow highlights the chemical shifts around 5.35 and 5.65 ppm to confirm the presence of acrylic protons of the methacrylate group, the green highlights at 2.9 ppm confirm the reduction of lysine methylene protons with increase of DM, and the blue highlights the new signal at 1.8 ppm assigned to the methyl moiety of the methacrylate.

trends to the hydrogel modulus and varied from ~7 (for G10P10) to ~28 (for G2P3) (Figure 2D). We saw a decrease in hydrogel swelling with increase in PEGDA concentration for the same GelMA concentration. The effect of PEGDA addition was more pronounced for the lower GelMA concentrations (G2 and G5) than the highest GelMA concentration (G10), where gels made with G10 also swelled less overall (Q_M of ~7–11) compared to gels made with G2 (Q_M of ~10–27) and G5 (Q_M of ~9–25).

We also investigated the stiffness of hydrogels made from GelMA of low DM (Supplementary Figure S1). As mentioned above, we classified G2P3 and G10 as soft hydrogels, while G2P10 and G10P10 were deemed stiff. It is worth noting that the low DM G2P3 was so soft that it presented difficulties when handling it during experiments. Our results showed that G10 of low DM had a Young's modulus of ~1 kPa. In contrast, both G10P10 and G2P10 showed a modulus of ~25 kPa, with no significant difference observed between them ($p > 0.05$). This data implies that the stiffness primarily arises from the PEGDA content, rather than the GelMA. Our results indicated that the degree of modification could be a useful strategy to manipulate hydrogel mechanical properties within a narrow range. For example, the same G10 gels were ~4 kPa for the high DM vs. ~1 kPa for the low DM GelMA and G10P10 gels were ~30 kPa for the high and ~25 kPa for the low DM GelMA (due to the overpowering effect of PEGDA on mechanical properties). Only high DM gels were used for further experiments as they allowed a broader range of mechanical properties and easier gel handling overall.

3.3 Hydrogel pore size and morphology

Figure 3A shows SEM images that highlight the structure of both the pure GelMA hydrogel (G10) and hybrid GelMA/PEGDA

10.3389/fbiom.2024.1408748

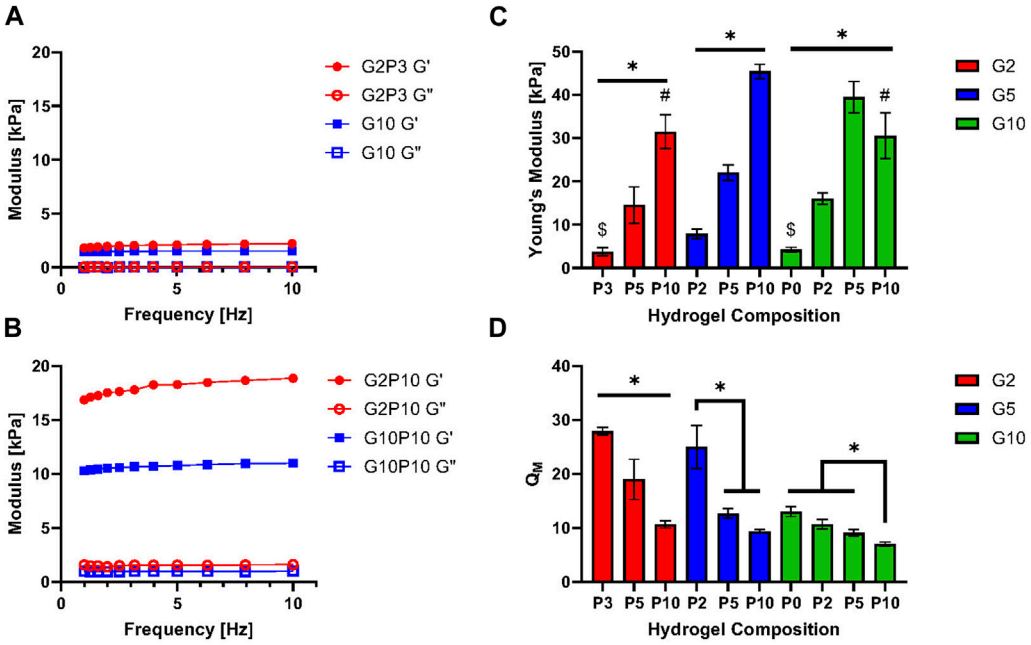

FIGURE 2
(A) Storage and loss moduli for the soft G2P3 and G10 GelMA/PEGDA hydrogels as a function of oscillation frequency. **(B)** Storage and loss moduli for stiff G2P10 and G10P10 GelMA/PEGDA hydrogels as a function of oscillation frequency. **(C)** Young's Modulus of GelMA/PEGDA hydrogels as a function of hydrogel composition. **(D)** Swelling ratio of GelMA/PEGDA hydrogels as a function of hydrogel composition. * Designates significant difference; one-way ANOVA test, $p < 0.05$, n = 3. # and $ designate no significant difference between denoted hydrogel pairs.

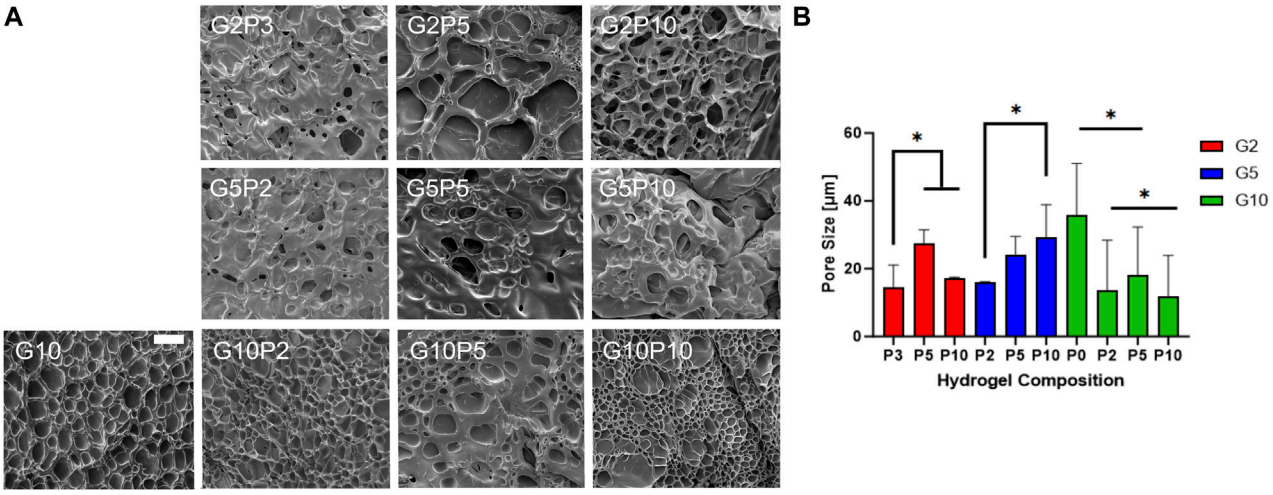

FIGURE 3
Characterization of hydrogel porosity. **(A)** Scanning electron microscope (SEM) images of all GelMA/PEGDA hydrogels. Scale bar = 50 μm. **(B)** Pore size measured from SEM images with the software ImageJ. * designates significant difference; one-way ANOVA test, $p < 0.05$, n = 3.

hydrogels. All gels exhibited an interconnected porous structure, where the pore size varied between ~9 (for G10P10)—~37 μm (for G10) (Figure 3B). Overall, the G10 gels appeared to have the most defined porous structure, while the addition of PEGDA seemed to lead to lower overall number of pores (for P2 and P3) or thicker walls (for P5 and P10), which could be attributed to higher crosslinking and is consistent with a higher gel modulus. Looking at the average pore size, G10 also seemed to have the highest pore size of all conditions of ~37 μm, suggesting the PEGDA addition led to a decrease in pore size. Further, the average pore size seemed to be higher for P5 gels than P2 or P3 gels for each GelMA concentration, suggesting that there might be an optimal PEGDA concentration that could lead to higher stiffness than GelMA gels alone, while also not compromising hydrogel porosity, where porosity is important for supporting cell growth.

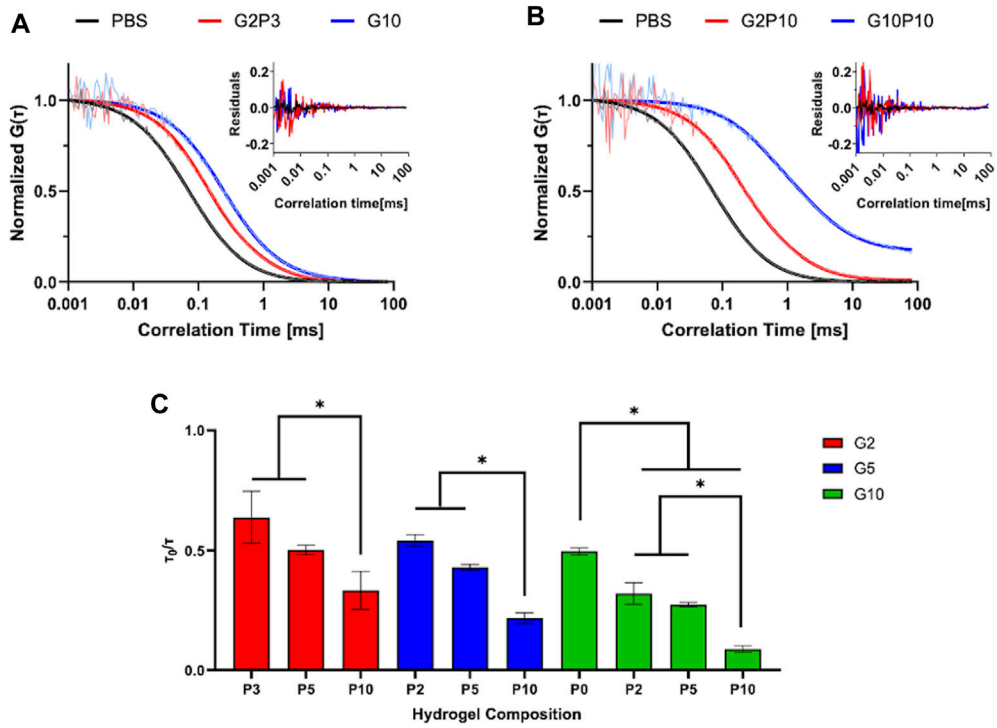

FIGURE 4
FCS Measurement of Diffusivity. Normalized autocorrelation curves of soft **(A)** and stiff **(B)** hydrogel pairs. Insets represent residuals of plotted data. **(C)** Measured normalized diffusivity of tested hydrogel conditions. * designates statistically significant difference between indicated groups. N = 4, $p < 0.05$.

3.4 Protein diffusivity in hydrogels as measured by fluorescence correlation spectroscopy

Fluorescence correlation spectroscopy (FCS) was used to measure diffusivity of a model protein RNase A as an indirect measure of hydrogel mesh size and porosity (Figure 4). As mesh size decreases, diffusivity would also be expected to decrease due to a more tortuous path through which the solute must diffuse. Hydrogels of varying compositions of GelMA and PEGDA were tested. Figures 4A,B show representative normalized autocorrelation functions and residuals (highlighting the goodness of the fit) for the soft and stiff hydrogel pairs of different GelMA concentrations. For all gels tested, we saw a shift of the autocorrelation function to the right compared to buffer only, indicative of slower solute diffusion in the hydrogels due to physical obstruction from polymer chains. Further, even though the soft and stiff gel pairs highlighted had the same modulus, they showed different protein diffusivity indicative of different porosity, corroborating the SEM observations of different pore structure between the gel pairs. For all tested conditions, protein diffusivity decreased (τ_0/τ decreased from ~0.5 to ~0.08) with increase in PEGDA concentration for the same GelMA concentration (Figure 4C). The diffusivity of the different hydrogels varied from τ_0/τ of 0.08 (for G10P10) to τ_0/τ of 0.64 (for G2P3). Overall, protein diffusivity trends tracked stiffness and swelling trends, where stiffer, less swollen gels showed lower diffusivity, indicative of higher crosslinking.

3.5 Detailed correlations of hydrogel composition and properties

We next aimed to clearly delineate the effect of PEGDA and GelMA independently as well as the total polymer concentration on the resultant hydrogel properties. To do so, we looked both at the total polymer concentration (Figures 5A–D) and at the GelMA fraction (Figures 5E–H). Overall, the hydrogel physical and mechanical properties showed a strong dependence on total polymer concentration and little to no correlation on the relative GelMA fraction. As expected, diffusivity and swelling decreased as total polymer concentration increased, while stiffness increased as a function of total polymer concentration. Pore size did not show nearly as strong of a correlation with total polymer concentration, potentially due to the sample preparation for SEM imaging. The relative amount of GelMA appeared to have no influence on hydrogel physical and mechanical properties, with R^2 values all less than 0.2. However, there was a weak correlation between GelMA fraction and hydrogel stiffness, where stiffness seemed to decrease with increase in GelMA fraction; however, there was a large data fluctuation (resulting in a low R^2 value) due to the pronounced effect of PEGDA on gel stiffness.

3.6 U87 cell viability and spreading in GelMA/PEGDA hydrogels

We first focused most of our analysis on two pairs of gels, the soft G10 and G2P3 and the stiff G2P10 and G10P10, representing the same

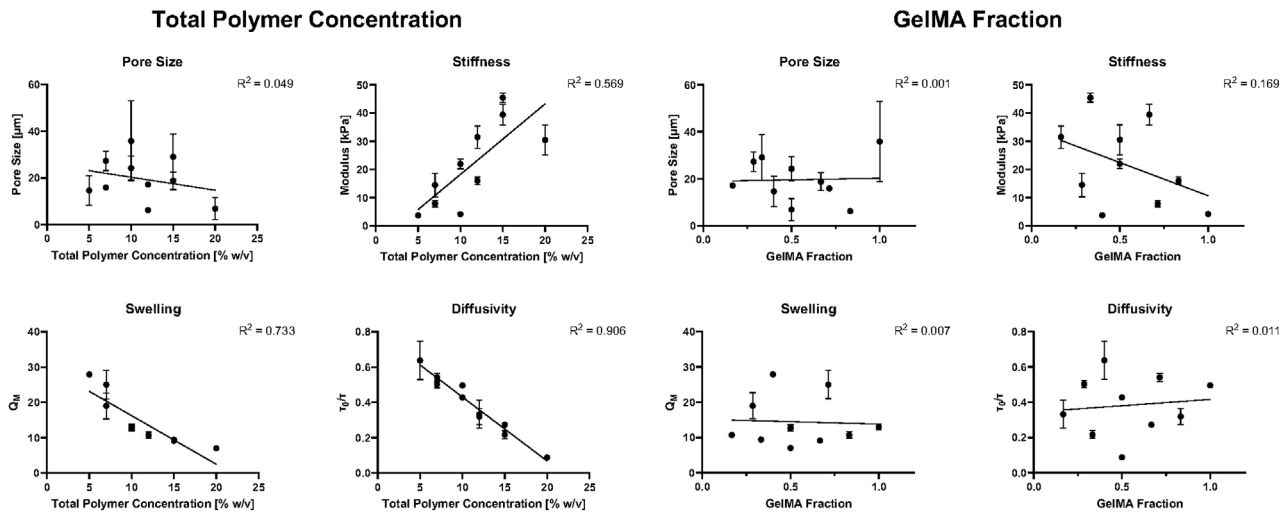

FIGURE 5
Hydrogel mechanical and physical properties as a function of total polymer concentration **(A–D)** and GelMA fraction **(E–H)**. A straight-line fit was used for all plots to show correlation.

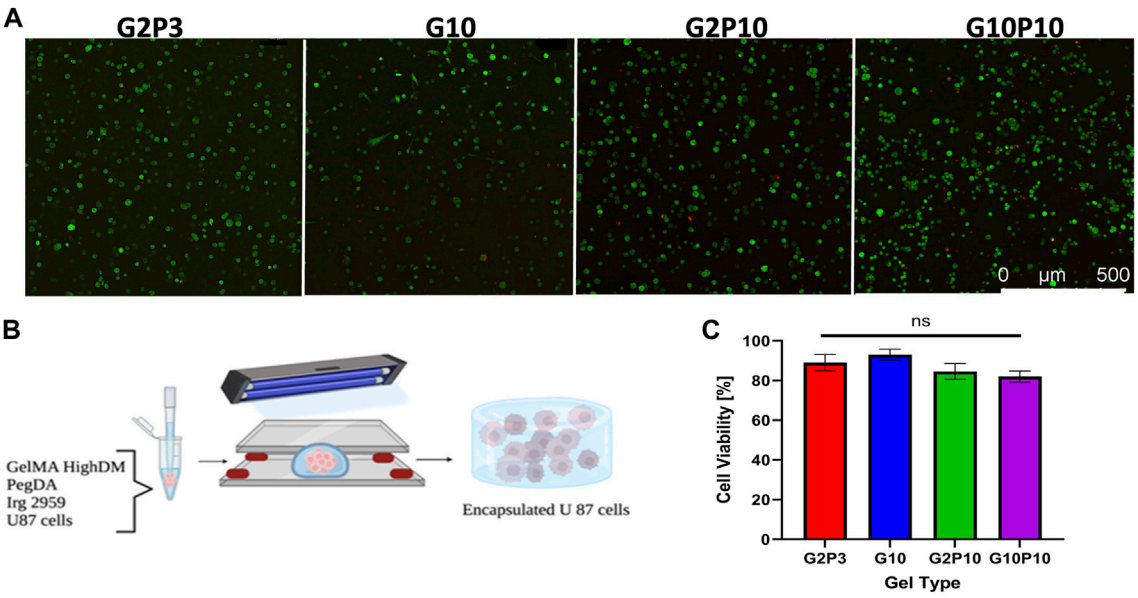

FIGURE 6
U87 Cell Viability within GelMA/PEGDA Hydrogels. **(A)** Representative confocal live/dead images of cells encapsulated in G2P3, G2P10, G10, and G10P10 hydrogels for 24 h. Acridine orange, AO (green stain) shows all cells and PI (red stain) shows dead cells. Scale bar = 100 μm. **(B)** Schematic of encapsulation of U87 cells in GelMA/PEGDA hydrogels. **(C)** Cell viability in the different hydrogel conditions on day 1 of culture (n = 3, $p < 0.5$).

stiffness but different biochemical properties. The gels also encompassed the 'extreme' of the tested gel formulations - from no PEGDA to maximum PEGDA and from minimum to maximum GelMA, to ascertain that the effect of both polymers is adequately represented. However, cell growth data are available for all gel conditions (Supplementary Figure S2 for images) and will be discussed further below. Here, we used U87 human glioblastoma cells as a model cell line because these cells are adhesion dependent, grow well in 3D culture and cell spreading upon adhesion is guided by the mechanical properties of the substrate as shown by us and others (Wang et al., 2014; Bruns et al., 2023). To further show that the gels are suitable for a variety of cell types, we also used NIH 3T3 normal mouse fibroblast cells, which have been used extensively in mechanosensing studies (Yu et al., 2020). For all conditions, cells were encapsulated during gelation and, hence, exposed to UV light (at 365 nm for 10 min) (Figure 6B). Consistent with our previous findings and those of others (Jung and Oh, 2014; Yue et al., 2015; Wang et al., 2018; Peter et al., 2019), the encapsulation procedure demonstrated no adverse effects on cell viability after 24 h (Figure 6A). In fact, we observed over 95% cell viability at the 24 h mark for both U87 cells (Figure 6C) and NIH 3T3 cells (Supplementary Figure S3),

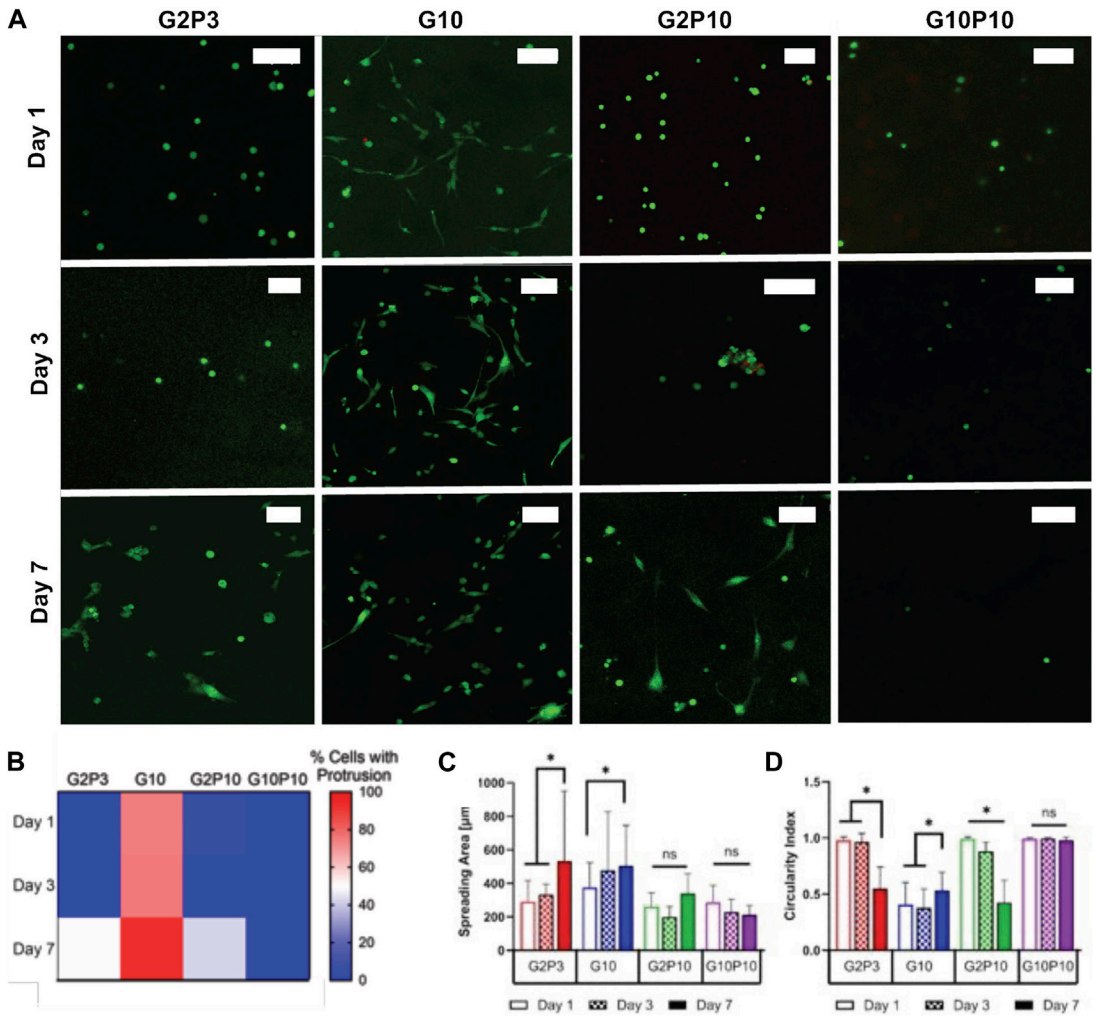

FIGURE 7
U87 glioblastoma cell spreading within GelMA/PEGDA hydrogels. **(A)** Fluorescent confocal z-stack images for tested conditions on Days 1, 3, and 7. Green cell tracker stains all cells. Scale bar represents 100 μm. **(B)**. Heat map of quantification of the percentage of cells that exhibited spreading on Day 1, 3, or 7. In this map, blue indicates areas where no spreading was observed (0% cells with protrusions), white corresponds to 50% spreading, and red signifies majority spreading. The color gradient allows for easy visualization of the distribution and extent of cell spreading over time. **(C)** Measured spreading area of cells within each condition as a function of time. **(D)** Calculated circularity index of measured conditions. * Indicates statistical significance between indicated groups (>120 cells/condition $p < 0.05$).

indicating the suitability of the developed materials as scaffolds for cell culture. Additionally, confocal imaging conducted at day 14 of culture revealed that the cells successfully infiltrated the entire hydrogel for both U87 cells (Supplementary Figure S4) and NIH 3T3 cells (Supplementary Figure S3).

We further evaluated cell spreading as a function of time for U87 cells only (Figure 7). Representative images of cells stained with cell tracker on days 1, 3 and 7 are shown in Figure 7A. We cultured all cells for 14 days (Supplementary Figure S4) but chose not to analyze individual cells for cell spreading area at day 14. However, qualitative observations showed that cells that did not spread by day 7 (e.g., cells in G10P10 gels) stayed round even on day 14. On the other hand, cells which spread early on (e.g., cells in G10 gels), had fully infiltrated the whole gel by day 14 (hence, it was technically difficult to quantify the spreading area of individual cells).

To better understand the time course of cells extending protrusions in the gels, we quantified the percentage of cells extending protrusions in each gel as a function of time (Supplementary Figure S2; Figure 7B). Overall, we noted that the pure GelMA gels (G10) allowed some cells to spread even at 24 h, while the addition of PEGDA in both the G2P3 and G2P10 gels delayed cell spreading until about day 7. Specifically, cells started to spread by day 6 in the G2P3 gels and by day 7 in the G2P10 gels (data now shown for all days for brevity). Cells were not able to extend protrusions in the G10P10 gels even at day 7 (and even at day 14 as shown in Supplementary Figure S3). Quantification of cell spreading area and circularity index corroborated our observations (Figures 7C,D). In G10 hydrogels cell area increased (from 375 to 477 μm^2) from day 1 to day 3, but did not change further by day 7, due to most cells being fully elongated by day 3. For cells in the G2P3 and G2P10 gels we noted an increase in cell spreading area and decrease in circularity at day 7 compared to days 1 and 3. No change was observed for cells in the G10P10 gels, where circularity was ~1 even at day 7, indicating lack of spreading.

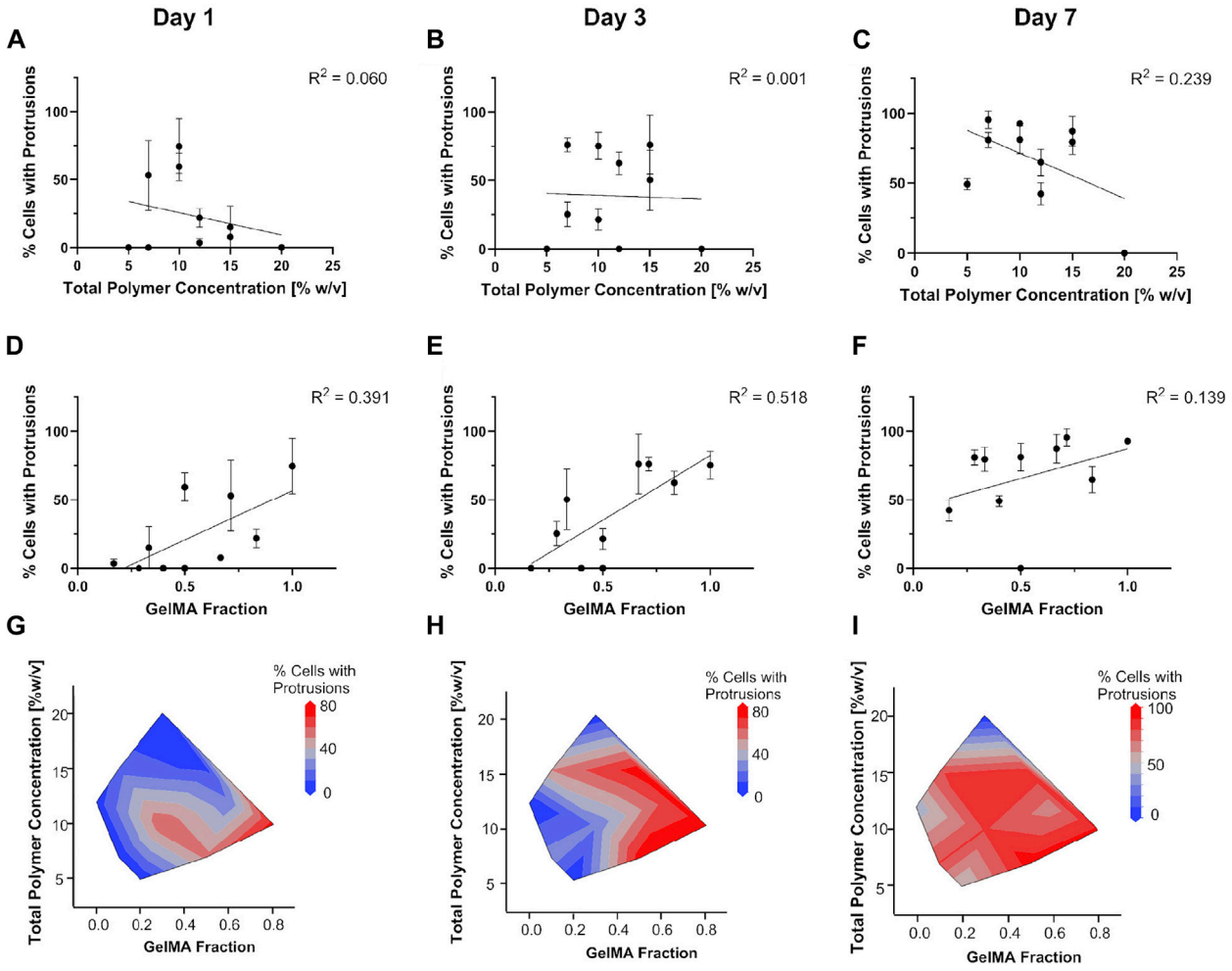

FIGURE 8
Dependence of U87 cell spreading on total polymer concentration **(A–C)** or GelMA fraction **(D–F)**. Contour plots in **(G–I)** detail the interplay in hydrogel stiffness and biochemical cues on cell spreading.

3.7 Detailed correlations of hydrogel composition/properties and cell spreading

To better understand cell spreading as a function of hydrogel composition and properties, we drew correlations between percentage of cells with protrusions and the total polymer concentration (which contributes to hydrogel stiffness) or GelMA fraction (which contributes to adhesion and degradation sites for cells) (Figure 8). For this analysis we looked at U87 cell spreading in all gel conditions (see cell images in Supplementary Figure S2). Our data showed that cell spreading was overall more dependent on the GelMA fraction as opposed to the total polymer concentration. The percentage of cells that exhibited spreading showed no correlation with total polymer concentration on Days 1 or 3. At day 7 total polymer concentration showed a weak correlation with cell spreading ($R^2 > 0.2$) (Figures 8A–C). On the other hand, GelMA fraction showed relatively clear correlation with cell spreading especially for days 1 and 3, with hydrogels with a higher proportion of GelMA exhibiting more spreading (Figures 8D–F). The trend was not as clear on Day 7 at which point cells were spread in most hydrogels. The data indicates that having a higher GelMA fraction (or concentration) leads to faster cell spreading independent of the total polymer concentration. Contour plots of the same data aided visualization (Figures 8G–I). They showed that initial cell spreading at day 1 was most pronounced for a high GelMA fraction (adhesion sites) and low total polymer concentration (gel stiffness). By day 3, the total polymer concentration (gel stiffness) did not show a pronounced impact, but GelMA fraction (adhesion sites) was still important. By day 7, the effect of both was masked as all cells, except for cells in G10P10, had spread.

3.8 Cell response to chemotherapeutics in GelMA/PEGDA hydrogels

We tested the effect of hydrogel composition on cell responsiveness to a chemotherapeutic. TMZ was chosen because it is the standard chemotherapy used for the treatment of glioblastoma. TMZ concentrations of 1–4 mM were chosen based on our preliminary work showing the IC_{50} (inhibitory concentration needed to kill 50% of cells) for U87 cells in 3D cell culture to be ~2 mM (Hill et al., 2021). The analysis of U87 cells' response to TMZ treatment demonstrated significant variability in cell viability across different hydrogel compositions. The confocal images in Supplementary Figure S5

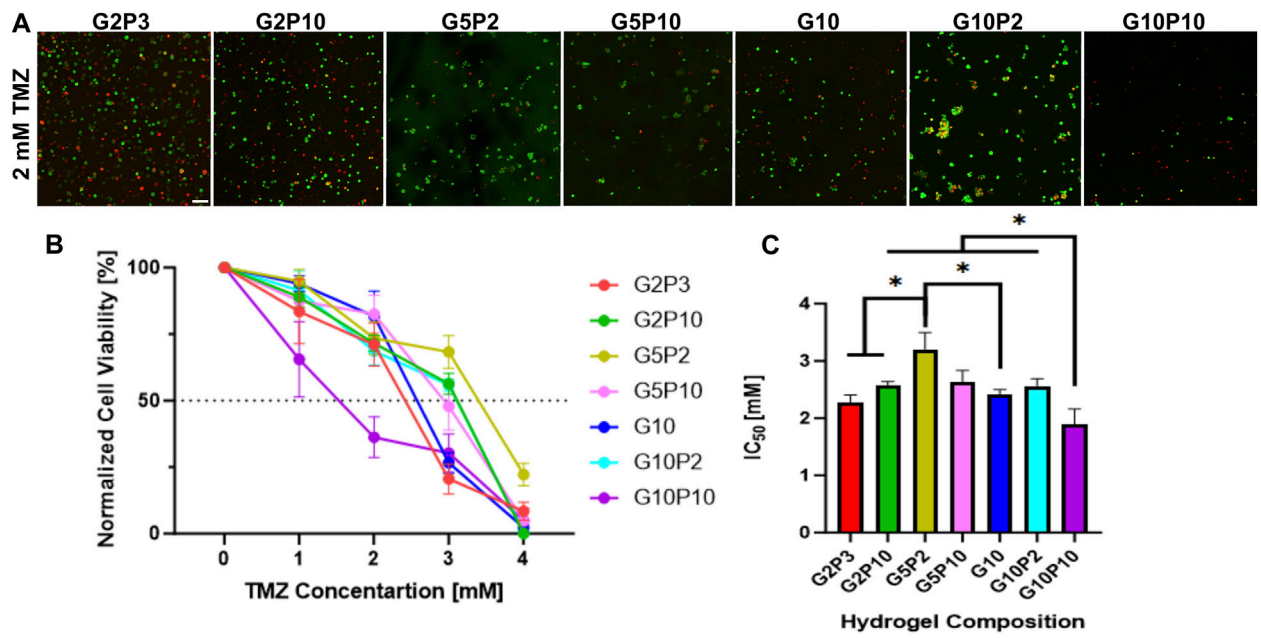

FIGURE 9
U87 cell response to TMZ treatment across various hydrogel compositions. **(A)** Fluorescent confocal Z stack images for all tested hydrogel compositions at 2 mM TMZ, the average IC_{50} concentration. Green fluorescence is cell tracker green, which stains all cells, while red fluorescence is propidium iodide, which stains dead cells. Scale bar is 100 μm. **(B)** Normalized percent cell viability across all hydrogel compositions at all tested TMZ concentrations (from 0 to 4 mM TMZ). Data points represent mean value with standard error. **(C)** Concentration of TMZ required to achieve 50% reduction in cell viability (IC_{50}) for each hydrogel composition tested. * Indicates statistical significance between indicated groups (n = 3, $p < 0.05$).

display all hydrogel compositions tested with TMZ concentrations ranging from 1 to 4 mM. 2 mM TMZ (Figure 9A) show a noticeable increase in the number of dead cells (red fluorescence) in certain hydrogel compositions compared to others. This observation was quantitatively supported by the cell viability data (Figure 9B), which illustrated a dose-dependent reduction in cell viability, with notable differences between the hydrogel compositions at higher TMZ concentrations. Figure 9C highlights the IC_{50} values for each hydrogel composition. The G5P2 hydrogel exhibited the highest IC_{50} value (~3.2 mM), indicating the least sensitivity to TMZ, whereas the G10P10 hydrogel had the lowest IC_{50} (~1.9 mM), indicating the highest sensitivity to TMZ. The results indicate that the response to TMZ did not correlate with PEGDA concentration. The IC_{50} concentration for the G5 hydrogel conditions was higher than that for both the G2 and G10 hydrogel conditions tested, irrespective of the PEGDA concentration. The IC_{50} showed a weak negative correlation with the total polymer concentration and no correlation with the GelMA fraction (Supplementary Figure S6).

4 Discussion

Here, we fabricated and characterized a library of GelMA/PEGDA hydrogels with the goal of achieving a highly tunable hydrogel system that allowed for the independent manipulation of hydrogel biochemical (i.e., cell adhesive and MMP-degradable sites) and mechanical (i.e., Young's modulus) properties for use in mechanosensing applications. The change in biochemical properties was achieved by varying the concentration of GelMA and the change in mechanical properties was achieved by varying the concentration of PEGDA. However, in varying the concentration of both polymers we also affected the total polymer concentration, which was expected to influence hydrogel pore size and permeability; hence, these properties were also measured. The effect of the gel properties on cell viability, spreading and drug responsiveness was then investigated. As a result, here we present a detailed analysis on the interplay between hydrogel composition-properties and their collective effect on cell viability, spreading and drug responsiveness. We used adhesion dependent cancerous U87 glioblastoma cells and normal NIH 3T3 fibroblast cells and focused on cell spreading since it is facilitated by integrin binding with adhesive ligands (e.g., RGD) present on GelMA, but not on PEGDA.

GelMA was synthesized in-house. When modifying gelatin with MAA to synthesize GelMA, the primary reaction is methacrylation of amino groups. However, at high MAA concentrations, esterification with hydroxyl groups may also occur, potentially altering GelMA properties (Shirahama et al., 2016). Despite the high MAA concentration used here, our ^{1}H NMR spectrum showed the absence of a peak at 4.0–4.5 ppm, indicating no esterification, and a visible vinyl proton at 5.5–6.5 ppm, confirming methacrylation. While most studies of GelMA hydrogels cite 50% degree of methacrylation (Nichol et al., 2010), we opted for a higher degree of 80%, aiming to enhance the stiffness of the resultant hydrogel (Figure 1). The selection of an 80% degree of methacrylation was influenced by studies indicating that higher degrees of methacrylation result in increased crosslink density and, consequently, a stiffer hydrogel network (Billiet et al., 2012; Malda et al., 2013). However, we confirmed that even a low degree of modification (i.e. 16%) could lead to gel formation but did not enable the same wide range of mechanical properties

(Supplementary Figure S1). We were concerned that while the methacrylation process does not directly modify cell binding sites (e.g., RGD), the overall conformational changes induced by methacrylation may impact the accessibility or functionality of RGD motifs and hence might negatively impact cell spreading (Xiao et al., 2019b). However, we noted excellent cell spreading in G10 only gels and with increase in GelMA concentration overall (as discussed below), negating these concerns. To obtain a wide range of stiffness with the high degree of modification GelMA, we combined GelMA at 2%–10% w/v with PEGDA at 2%–10% w/v, giving Young's moduli in the range of ~3–43 kPa (Figure 2).

The change in polymer concentration affected other hydrogel properties such as porosity as measured via SEM (Figure 3). We did not observe an overall correlation between modulus and porosity and noted that all gels exhibited a porous structure necessary for cell growth. However, at least for the 5% w/v GelMA we noted an increase in pore size with increase in PEGDA concentration (despite a corresponding increase in modulus and decrease in swelling). Corroborating this observation, a prior study by Wang et al. found that adding 5% PEGDA to a GelMA gel substantially increased the gel pore diameter (Wang et al., 2018). This observation was also consistent with our findings in the G2 and G5 samples for all PEGDA concentrations, but inconsistent with our observation of the highest overall porosity for the G10 gels containing no PEGDA.

The change in polymer concentration affected hydrogel swelling (Figure 2D) and permeability as estimated via FCS measurement of diffusivity of a fluorescent protein in the gels (Figure 4). Both properties, swelling and permeability, were inversely correlated with gel modulus. The decrease in diffusivity with increase in polymer concentration could be attributed to a higher degree of crosslinking, which appeared driven predominantly by the addition of PEGDA and minimally affected by the GelMA concentration. Similar trends were noted by Dogan et al., who noted that the diffusivity of solutes inside GelMA hydrogels was influenced more strongly by the degree of methacrylation (i.e., crosslinking density) as opposed to the total GelMA concentration for the same degree of crosslinking (Dogan et al., 2023). However, Pedron et al. showed that both degree of methacrylation and total polymer content led to changes in diffusivity, with a more pronounced drop in diffusivity for the high GelMA concentration of 10% w/v (compared to 5% or 7% w/v) (Pedron and Harley, 2013).

Gel permeability (i.e., diffusivity measured via FCS) correlated with gel pore size with some exceptions, such as, for example, G10P2 compared to G10P5, which had similar diffusivity even though G10P2 had smaller pore size compared to G10P5. We suggest that this seeming discrepancy is related to the hydrogels' morphology and the nature of the SEM vs. FCS measurements. SEM provides valuable data of gel morphology, but requires gel freezing and freeze-drying, which could disrupt the gel structure and result in pore sizes higher than those observed in the gel hydrated state (Bruns et al., 2018). FCS measures diffusivity of gels in their natural equilibrium hydrated state, where diffusivity would depend on pore size, pore number, pore interconnectivity and wall thickness. Lower pore number and interconnectivity and higher wall thickness would all lead to a higher tortuosity of the path length for a diffusing molecule, leading to lower diffusivity. Our quantitative data shows a lower pore size for G10P2 compared to G10P10, which should have resulted in lower diffusivity for G10P2. However, qualitatively we noted lower wall thickness and higher number of pores in the G10P2 compared to G10P5 gels, possibly negating the effect of the smaller pore size and resulting in similar diffusivity.

Our results indicate that for each GelMA concentration, the addition of PEGDA led to a higher degree of crosslinking and a higher modulus. For example, in Figure 5, we showed a strong correlation between total polymer concentration and modulus, where the modulus increased with increase in total polymer concentration. At the same time, there was a weak negative correlation between GelMA fraction and modulus, showing that as the GelMA concentration increased, modulus decreased. Hence, the hydrogel modulus was governed primarily by the PEGDA concentration. Overall, while a strong correlation was found between gel mechanical and physical properties and total polymer concentration, the fraction of GelMA used in the composite gels did not have a pronounced effect on gel properties (Figure 5).

The GelMA/PEGDA encapsulation process ensured uniform cell distribution, with consistently high >90% cell viability for different cell types (Figures 6, 9; Supplementary Figure S3). However, cell spreading was dependent on hydrogel composition, where it increased with increase in GelMA and decreased with increase in total polymer concentration (Figure 9). These variations in cell spreading dynamics across different hydrogel formulations suggest that distinct matrix properties influence cellular behaviors (Figure 7). Cell spreading dynamics proved to be more dependent on the relative GelMA to PEGDA fraction than on total polymer concentration. Cell spreading exhibited no correlation with total polymer concentration on Days 1 or 3, while GelMA fraction demonstrated a clear correlation with increased cell spreading. Although less distinct on Days 3 and 7, the data suggests that higher GelMA fractions led to faster cell spreading. Overall, our results showed that when the PEGDA concentration was kept at or below 10% w/v (except for G10P10), all gels were able to support cell spreading, albeit at different times. However, adding any PEGDA led to slower cell spreading with just a few cells showing protrusions at 24 h even for the lowest PEGDA concentrations tested, compared to most cells showing protrusions in the GelMA only gels. Similar results were observed by Mahdavi et al. (2021), where the authors reported that adding PEGDA might delay cell proliferation and growth compared to GelMA alone for 3D encapsulation of corneal stromal cells. However, Wang et al. (2018) showed that 2D cultures of mouse osteoblast MC23T3-E1 cells exhibited high viability, adhesion, and proliferation in both GelMA alone at concentrations of 10%, 20%, and 30%, as well as in the same concentrations of GelMA with an additional 5% PEGDA, indicating that the effect of PEGDA on cell spreading might be specific to 3D cell culture. Others have also shown that cell spreading correlates with GelMA concentration and that a high amount of polymer and crosslinking (as in G10P10) could prevent spreading. For example, Peter et al. have shown that MDA-MB-231 breast cancer cells develop a spindle-shaped morphology in GelMA-rich hydrogels, but retain a spheroidal morphology in PEGDA rich gels (PEGDA >15% w/v) (Peter et al., 2019).

Overall, the higher concentration of cell-adhesion (e.g., RGD) and MMP-degradable moieties in G10 gels (except for G10P10) promoted cell attachment. For example, although G2P3 and G10 gels shared similar stiffness, G10, with five times more binding sites, promoted

better cell attachment and spreading. In G2P3, while cells could adhere, they required additional time to remodel the scaffold and access sparser binding sites compared to G10. G2P10, although stiffer than G2P3, contained an equivalent number of binding sites. The increased PEGDA content in G2P10 reduced pore size and lowered the diffusion coefficient by two-fold, yet cells were able to spread within a comparable timeframe in both conditions. These findings underscore the nuanced interplay between hydrogel composition, stiffness, binding sites, and diffusion properties, influencing cell spreading dynamics in 3D culture systems. The only hydrogel that did not support cell spreading at 7 days and even at 14 days was the G10P10 gel (Supplementary Figures S2, S3, S4), which was attributed to its low diffusivity and smaller pore size. Qualitative observations showed that cells did not increase in number over time in those gels, indicative of impeded cell proliferation and possibly cell death after 24 h. One limitation for those gels was the high viscosity of the gel precursor solution due to the high total polymer concentration, which led to difficulties in pipetting and sometimes resulted in air bubbles being trapped in the gel (where the high surface tension of the air bubbles could explain a lower cell viability). Hence, the G10P10 gel was the upper limit of total polymer concentration that was practical for cell encapsulation.

Lastly, we tested the effect of hydrogel composition on U87 cell responsiveness to TMZ treatment. TMZ is the chemotherapeutic of choice for the treatment of GBM, although it has limited effectiveness and high toxicity (Janjua et al., 2021). 3D cell culture, and hydrogels in particular, have emerged as promising *in vitro* platforms for drug screening applications because they can be adapted to existing high-throughout screening technologies, while mimicking the physiological environment more faithfully than a standard 2D cell culture (Zustiak, 2015). Our results showed that within the conditions tested here, there was no clear correlation between cell responsiveness to TMZ and total polymer concentration or GelMA fraction (Figure 9; Supplementary Figures S5, S6). However, the condition G5P2 showed significantly higher IC_{50} than all other conditions, while the condition G10P10 showed significantly lower IC_{50} than all other conditions. G5P2 has a medium GelMA concentration and low PEGDA and total polymer concentration and G10P10 had the highest total polymer concentration tested. While more studies are needed, our data suggest that there might be an optimal number of adhesive sites and hydrogel properties such as swelling, stiffness and diffusivity (Figure 5) that confer resistance to TMZ treatment. Our findings suggest that hydrogel composition could influence the therapeutic effectiveness of TMZ in U87 GBM cells, which could inform future design strategies for hydrogel-based drug screening platforms.

Collectively, our results indicate that the developed hydrogel formulations are suitable for mechanosensting applications with some limitations. Among the design parameters important for hydrogels used in mechanosensing studies, are a wide range of mechanical properties and independent tunability of mechanical, biochemical and physical properties. The latter is an especially important consideration for 3D cell cultures, where cells are embedded inside the hydrogels. The GelMA/PEGDA hydrogels described here cover a wide range of moduli, from ~3 to ~45 kPa, which encompasses the moduli of most soft tissues in the body (Levental et al., 2007). Further, they allow for independent tuning of mechanical and biochemical properties, where formulations of similar modulus but different biochemical properties and similar biochemical properties but different modulus were identified. While porosity and diffusivity of the hydrogels were also affected by the chemical composition, we saw a ~15-fold change in modulus (for the tested formulations) compared to only a ~3-fold change in pore size and diffusivity. Further, the average pore size was >10 μm for all hydrogel compositions and even hydrogels with high PEGDA concentrations and high modulus (e.g., G5P10, E = 45.7 ± 1.6 kPa) exhibited some of the highest pore sizes of ~30 μm. Pore sizes greater than the typical cell size (~10 μm) are optimal to allow for cell spreading and proliferation (Loh and Choong, 2013). The diffusivity of macromolecules in the hydrogels was linearly dependent on total polymer concentration, but it was impeded by up to 70% even at the highest polymer concentration used. Lastly, while the addition of PEGDA delayed cell spreading, cell spreading and protrusions were seen for all hydrogel formulations by day 3 (except for G10P10 as described earlier). The gels retained their integrity over a long period, but cell culture was terminated at 14 days because most gels were fully infiltrated with cells by that time point. However, longer time points could be pursued if needed for different applications.

5 Conclusion

This study explores the intricate interplay of biochemical and mechanical properties within GelMA/PEGDA hydrogels, offering insights into the influence of total polymer concentration and the GelMA/PEGDA ratio, with a specific focus on their impact on hydrogel properties and subsequent cell spreading and drug responsiveness. Our findings reveal a robust dependence of hydrogel properties, such as modulus, swelling, pore size, and permeability, on total polymer concentration, while indicating minimal correlation with the relative GelMA/PEGDA ratio. At the same time, the amount of GelMA had a more profound effect on cell spreading than the total polymer concentration and any addition of PEGDA delayed cell spreading until about day 3 of culture. Drug responsiveness showed a weak negative correlation with total polymer concentration and no correlation with the GelMA fraction, although one condition, namely, G5P2, exhibited the highest IC_{50}. Further, we showcased GelMA/PEGDA composition pairs, namely, the soft G2P3 and G10, ~3 kPa in Young's modulus, vs. the stiff G2P10 and G10P10, ~35 kPa in Young's modulus, which exhibited similar stiffness but different number of adhesive sights or different stiffness but the same number of adhesive sites. This diversity in properties emphasizes the versatility of the GelMA/PEGDA hydrogel system, suggesting its potential suitability for mechanosensing studies.

Data availability statement

The raw data supporting the conclusions of this article will be made available by the authors, without undue reservation.

Author contributions

EF: Conceptualization, Methodology, Writing–original draft, Writing–review and editing, Data curation, Formal Analysis,

Investigation. SS: Data curation, Formal Analysis, Investigation, Writing–review and editing. PB: Data curation, Formal Analysis, Writing–review and editing, Software. SZ: Writing–review and editing, Conceptualization, Funding acquisition, Methodology, Project administration, Resources, Supervision, Writing–original draft.

Funding

The author(s) declare that financial support was received for the research, authorship, and/or publication of this article. Funding for this work was partially provided by major research infrastructure grant 1920251 from the National Science Foundation awarded to SPZ. Funding was also partially provided by a graduate assistantship awarded to EF by the School of Science and Engineering, Saint Louis University.

Acknowledgments

We would like to thank Nathaniel Huebsch and Harper Jiang for advice on GelMA synthesis. We thank Fahu He for help and training on the nuclear magnetic resonance.

Conflict of interest

The authors declare that the research was conducted in the absence of any commercial or financial relationships that could be construed as a potential conflict of interest.

The author(s) declared that they were an editorial board member of Frontiers, at the time of submission. This had no impact on the peer review process and the final decision.

Publisher's note

Supplementary material

The Supplementary Material for this article can be found online at: https://www.frontiersin.org/articles/10.3389/fbiom.2024.1408748/full#supplementary-material

References

Billiet, T., Vandenhaute, M., Schelfhout, J., Van Vlierberghe, S., and Dubruel, P. (2012). A review of trends and limitations in hydrogel-rapid prototyping for tissue engineering. *Biomaterials* 33 (26), 6020–6041. doi:10.1016/j.biomaterials.2012.04.050

Bruns, J., Egan, T., Mercier, P., and Zustiak, S. P. (2023). Glioblastoma spheroid growth and chemotherapeutic responses in single and dual-stiffness hydrogels. *Acta Biomater.* 163, 400–414. doi:10.1016/j.actbio.2022.05.048

Bruns, J., McBride-Gagyi, S., and Zustiak, S. P. (2018). Injectable and cell-adhesive polyethylene glycol cryogel scaffolds: independent control of cryogel microstructure and composition. *Macromol. Mater. Eng.* 303 (10), 1800298. doi:10.1002/mame.201800298

Caliari, S. R., and Burdick, J. A. (2016). A practical guide to hydrogels for cell culture. *Nat. methods* 13 (5), 405–414. doi:10.1038/nmeth.3839

Claaßen, C., Claaßen, M. H., Truffault, V., Sewald, L., Tovar, G. E., Borchers, K., et al. (2018). Quantification of substitution of gelatin methacryloyl: best practice and current pitfalls. *Biomacromolecules* 19 (1), 42–52. doi:10.1021/acs.biomac.7b01221

Dogan, E., Holshue, C., Bhusal, A., Shukla, R., and Miri, A. K. (2023). Cell encapsulation in gelatin methacryloyl bioinks impairs microscale diffusion properties. *Front. Bioeng. Biotechnol.* 11, 1193970. doi:10.3389/fbioe.2023.1193970

Dong, X., Sun, Q., Geng, J., Liu, X., and Wei, Q. (2024). Fiber flexibility reconciles matrix recruitment and the fiber modulus to promote cell mechanosensing. *Nano Lett.* 24 (13), 4029–4037. doi:10.1021/acs.nanolett.4c00923

Duan, J., Cao, Y., Shen, Z., Cheng, Y., Ma, Z., Wang, L., et al. (2022). 3D bioprinted GelMA/PEGDA hybrid scaffold for establishing an *in vitro* model of melanoma. *J. Microbiol. Biotechnol.* 32 (4), 531–540. doi:10.4014/jmb.2111.11003

Dutta, R. C., and Dutta, A. K. (2009). Cell-interactive 3D-scaffold; advances and applications. *Biotechnol. Adv.* 27 (4), 334–339. doi:10.1016/j.biotechadv.2009.02.002

Hill, L., Bruns, J., and Zustiak, S. P. (2021). Hydrogel matrix presence and composition influence drug responses of encapsulated glioblastoma spheroids. *Acta Biomater.* 132, 437–447. doi:10.1016/j.actbio.2021.05.005

Hoch, E., Schuh, C., Hirth, T., Tovar, G. E., and Borchers, K. (2012). Stiff gelatin hydrogels can be photo-chemically synthesized from low viscous gelatin solutions using molecularly functionalized gelatin with a high degree of methacrylation. *J. Mater. Sci. Mater. Med.* 23 (11), 2607–2617. doi:10.1007/s10856-012-4731-2

Huang, G., Li, F., Zhao, X., Ma, Y., Li, Y., Lin, M., et al. (2017). Functional and biomimetic materials for engineering of the three-dimensional cell microenvironment. *Chem. Rev.* 117 (20), 12764–12850. doi:10.1021/acs.chemrev.7b00094

Hutson, C. B., Nichol, J. W., Aubin, H., Bae, H., Yamanlar, S., Al-Haque, S., et al. (2011). Synthesis and characterization of tunable poly (ethylene glycol): gelatin methacrylate composite hydrogels. *Tissue Eng. Part A* 17 (13-14), 1713–1723. doi:10.1089/ten.tea.2010.0666

Janjua, T. I., Rewatkar, P., Ahmed-Cox, A., Saeed, I., Mansfeld, F. M., Kulshreshtha, R., et al. (2021). Frontiers in the treatment of glioblastoma: past, present and emerging. *Adv. drug Deliv. Rev.* 171, 108–138. doi:10.1016/j.addr.2021.01.012

Jiang, T., Zhao, J., Yu, S., Mao, Z., Gao, C., Zhu, Y., et al. (2019). Untangling the response of bone tumor cells and bone forming cells to matrix stiffness and adhesion ligand density by means of hydrogels. *Biomaterials* 188, 130–143. doi:10.1016/j.biomaterials.2018.10.015

Jung, J., and Oh, J. (2014). Swelling characterization of photo-cross-linked gelatin methacrylate spherical microgels for bioencapsulation. *e-Polymers* 14 (3), 161–168. doi:10.1515/epoly-2014-0025

Kim, B.-S., Nikolovski, J., Bonadio, J., Smiley, E., and Mooney, D. J. (1999). Engineered smooth muscle tissues: regulating cell phenotype with the scaffold. *Exp. Cell Res.* 251 (2), 318–328. doi:10.1006/excr.1999.4595

Lepedda, A. J., Nieddu, G., Formato, M., Baker, M. B., Fernandez-Perez, J., and Moroni, L. (2021). Glycosaminoglycans: from vascular physiology to tissue engineering applications. *Front. Chem.* 9, 680836. doi:10.3389/fchem.2021.680836

Levental, I., Georges, P. C., and Janmey, P. A. (2007). Soft biological materials and their impact on cell function. *Soft Matter* 3 (3), 299–306. doi:10.1039/b610522j

Liu, Y., Zhang, J., Jin, Y., and Yin, M. (2024). Gelatin methacrylate based liquid dressing with antibacterial and hemostasis properties. *Colloids Surfaces A Physicochem. Eng. Aspects* 689, 133749. doi:10.1016/j.colsurfa.2024.133749

Loessner, D., Meinert, C., Kaemmerer, E., Martine, L. C., Yue, K., Levett, P. A., et al. (2016). Functionalization, preparation and use of cell-laden gelatin methacryloyl–based hydrogels as modular tissue culture platforms. *Nat. Protoc.* 11 (4), 727–746. doi:10.1038/nprot.2016.037

Loh, Q. L., and Choong, C. (2013). Three-dimensional scaffolds for tissue engineering applications: role of porosity and pore size. *Tissue Eng. Part B Rev.* 19, 485–502. doi:10.1089/ten.teb.2012.0437

Mahdavi, S. S., Abdekhodaie, M. J., Mashayekhan, S., Baradaran-Rafii, A., and Kim, K. (2021). Development and *in vitro* evaluation of photocurable GelMA/PEGDA hybrid hydrogel for corneal stromal cells delivery. *Mater. Today Commun.* 27, 102459. doi:10.1016/j.mtcomm.2021.102459

Malda, J., Visser, J., Melchels, F. P., Jüngst, T., Hennink, W. E., Dhert, W. J., et al. (2013). 25th anniversary article: engineering hydrogels for biofabrication. *Adv. Mater.* 25 (36), 5011–5028. doi:10.1002/adma.201302042

Mamaghani, K. R., Naghib, S. M., Zahedi, A., and Mozafari, M. (2018). Synthesis and microstructural characterization of GelMa/PEGDA hybrid hydrogel containing graphene oxide for biomedical purposes. *Mater. Today Proc.* 5 (7), 15635–15644. doi:10.1016/j.matpr.2018.04.173

Nichol, J. W., Koshy, S. T., Bae, H., Hwang, C. M., Yamanlar, S., and Khademhosseini, A. (2010). Cell-laden microengineered gelatin methacrylate hydrogels. *Biomaterials* 31 (21), 5536–5544. doi:10.1016/j.biomaterials.2010.03.064

O'Connell, C. D., Zhang, B., Onofrillo, C., Duchi, S., Blanchard, R., Quigley, A., et al. (2018). Tailoring the mechanical properties of gelatin methacryloyl hydrogels through manipulation of the photocrosslinking conditions. *Soft matter* 14 (11), 2142–2151. doi:10.1039/c7sm02187a

Pedron, S., and Harley, B. (2013). Impact of the biophysical features of a 3D gelatin microenvironment on glioblastoma malignancy. *J. Biomed. Mater. Res. Part A* 101 (12), 3404–3415. doi:10.1002/jbm.a.34637

Pepelanova, I., Kruppa, K., Scheper, T., and Lavrentieva, A. (2018). Gelatin-methacryloyl (GelMA) hydrogels with defined degree of functionalization as a versatile toolkit for 3D cell culture and extrusion bioprinting. *Bioengineering* 5 (3), 55. doi:10.3390/bioengineering5030055

Peter, M., Singh, A., Mohankumar, K., Jeenger, R., Joge, P. A., Gatne, M. M., et al. (2019). Gelatin-based matrices as a tunable platform to study *in vitro* and *in vivo* 3D cell invasion. *ACS Appl. Bio Mater.* 2 (2), 916–929. doi:10.1021/acsabm.8b00767

Shirahama, H., Lee, B. H., Tan, L. P., and Cho, N.-J. (2016). Precise tuning of facile one-pot gelatin methacryloyl (GelMA) synthesis. *Sci. Rep.* 6 (1), 31036. doi:10.1038/srep31036

Sun, M., Sun, X., Wang, Z., Guo, S., Yu, G., and Yang, H. (2018a). Synthesis and properties of gelatin methacryloyl (GelMA) hydrogels and their recent applications in load-bearing tissue. *Polymers* 10 (11), 1290. doi:10.3390/polym10111290

Sun, Y., Deng, R., Ren, X., Zhang, K., and Li, J. (2018b). 2D gelatin methacrylate hydrogels with tunable stiffness for investigating cell behaviors. *ACS Appl. Bio Mater.* 2 (1), 570–576. doi:10.1021/acsabm.8b00712

Theocharis, A. D., Skandalis, S. S., Gialeli, C., and Karamanos, N. K. (2016). Extracellular matrix structure. *Adv. drug Deliv. Rev.* 97, 4–27. doi:10.1016/j.addr.2015.11.001

Tibbitt, M. W., and Anseth, K. S. (2009). Hydrogels as extracellular matrix mimics for 3D cell culture. *Biotechnol. Bioeng.* 103 (4), 655–663. doi:10.1002/bit.22361

Tomal, W., and Ortyl, J. (2020). Water-soluble photoinitiators in biomedical applications. *Polymers* 12 (5), 1073. doi:10.3390/polym12051073

Van Den Bulcke, A. I., Bogdanov, B., De Rooze, N., Schacht, E. H., Cornelissen, M., and Berghmans, H. (2000). Structural and rheological properties of methacrylamide modified gelatin hydrogels. *Biomacromolecules* 1 (1), 31–38. doi:10.1021/bm990017d

Vila, A., Torras, N., Castaño, A. G., García-Díaz, M., Comelles, J., Pérez-Berezo, T., et al. (2020). Hydrogel co-networks of gelatine methacrylate and poly (ethylene glycol) diacrylate sustain 3D functional *in vitro* models of intestinal mucosa. *Biofabrication* 12 (2), 025008. doi:10.1088/1758-5090/ab5f50

Walker, C., Mojares, E., and del Río Hernández, A. (2018). Role of extracellular matrix in development and cancer progression. *Int. J. Mol. Sci.* 19 (10), 3028. doi:10.3390/ijms19103028

Wang, C., Tong, X., and Yang, F. (2014). Bioengineered 3D brain tumor model to elucidate the effects of matrix stiffness on glioblastoma cell behavior using PEG-based hydrogels. *Mol. Pharm.* 11 (7), 2115–2125. doi:10.1021/mp5000828

Wang, Y., Ma, M., Wang, J., Zhang, W., Lu, W., Gao, Y., et al. (2018). Development of a photo-crosslinking, biodegradable GelMA/PEGDA hydrogel for guided bone regeneration materials. *Materials.* 11 (8), 1345. doi:10.3390/ma11081345

Xiao, S., Zhao, T., Wang, J., Wang, C., Du, J., Ying, L., et al. (2019a). Gelatin methacrylate (GelMA)-based hydrogels for cell transplantation: an effective strategy for tissue engineering. *Stem Cell Rev. Rep.* 15, 664–679. doi:10.1007/s12015-019-09893-4

Xiao, S., Zhao, T., Wang, J., Wang, C., Du, J., Ying, L., et al. (2019b). Gelatin methacrylate (GelMA)-based hydrogels for cell transplantation: an effective strategy for tissue engineering. *Stem Cell Rev. Rep.* 15, 664–679. doi:10.1007/s12015-019-09893-4

Yu, L., Hou, Y., Xie, W., Camacho, J. L. C., Cheng, C., Holle, A., et al. (2020). Ligand diffusion enables force-independent cell adhesion via activating α5β1 integrin and initiating rac and RhoA signaling. *Adv. Mater.* 32 (29), 2002566. doi:10.1002/adma.202002566

Yue, K., Trujillo-de Santiago, G., Alvarez, M. M., Tamayol, A., Annabi, N., and Khademhosseini, A. (2015). Synthesis, properties, and biomedical applications of gelatin methacryloyl (GelMA) hydrogels. *Biomaterials* 73, 254–271. doi:10.1016/j.biomaterials.2015.08.045

Zustiak, S. P. (2015). The role of matrix compliance on cell responses to drugs and toxins: towards predictive drug screening platforms. *Macromol. Biosci.* 15 (5), 589–599. doi:10.1002/mabi.201400507